

Comparative study on morphological skeletonization and fuzzy medial axis transformation*

Sen-Ren Jan

Ming-Hsin Institute of Technology
Department of Information Management
Hsinchu, Taiwan 304, Republic of China

Yuang-Cheh Hsueh

National Chiao-Tung University
Department of Computer and Information Science
Hsinchu, Taiwan 300, Republic of China
E-mail: ychsueh@cis.nctu.edu.tw

Abstract. *In this paper, we make a comparative study on morphological skeletonization (MSK) and fuzzy medial axis transformation (FMAT). Methods have been proposed to construct convex FMAT from the morphological skeleton points and to translate FMAT to MSK, respectively. For the case of translating MSK to convex FMAT, the experimental results reveal that the combination of the proposed method and the redundant removal algorithm is very effective. Especially, the combined method is faster than the original method for constructing convex FMAT of smoothed images. © 2002 SPIE and IS&T. [DOI: 10.1117/1.1426075]*

1 Introduction

The skeleton transformation is a generally used geometrical shape representation in a computer vision system. The skeleton transformation can reduce the time and storage needed for further computer processing. In the last decade, mathematical morphology¹ has been an useful tool for many problems of the digital image processing, e.g., segmentation, thinning, or skeletonization. Meanwhile, the fuzzy set theory has been found a promising field of application in digital image processing.^{2–9} The fuzzy set theory ideally fits human intuitive knowledge of the diffuse localization or limits of the image components. It is usually used to model uncertainty and imprecision of the image components. Recently, several attempts^{2,10–12} have been made to build a mathematical morphology relying on intrinsically fuzzy approaches. These interesting approaches motivated us to investigate the relations between morphological skeletonization and fuzzy medial axis transformation.

*This work was supported partially by the National Science Council, Republic of China, under Grant No. NSC 87-2213-E-009-010.

Paper 99065 received Nov. 15, 1999; revised manuscript received Apr. 17, 2001; accepted for publication April 26, 2001.
1017-9909/2002/\$15.00 © 2002 SPIE and IS&T.

It is well known that skeletons of binary images are defined by the notion of maximal disks.¹³ Based on this notion, morphological skeletonization (MSK) is developed and generalized^{1,14–20} to find skeletons of gray-scale images. On the other hand, based on the notion of maximum fuzzy disks, fuzzy medial axis transformation (FMAT) is proposed to find the fuzzy medial axis of gray-scale images.^{21,22} Although both MSK and FMAT originated from the notion of maximal disks, the morphological skeleton and the fuzzy medial axis of a gray-scale image are not the same. Therefore, it is our purpose in this paper to make a comparative study on MSK and FMAT. In next section, we will briefly review the concepts of MSK and FMAT. In Sec. 3, we will compare them and explore their relations. In Sec. 4, we will propose the translation methods between the convex FMAT and the MSK of an image. In Sec. 5, we will show and discuss some experimental results on constructing convex FMAT from the MSK. Finally, in Sec. 6, we will make some conclusions.

2 Morphological Skeletonization and FMAT

2.1 Morphological-Skeletonization MSK

The four basic morphological operations dilation, erosion, closing, and opening are usually denoted by \oplus , \ominus , \bullet , and \circ , respectively. Then the morphological skeleton $SK_B(X)$ of a discrete binary image X with respect to a discrete structuring element B is defined^{1,15} as follows:

$$SK_B^{(n)}(X) = [X \ominus nB] \setminus [(X \ominus nB) \circ B], \quad n = 0, 1, \dots \quad (1)$$

$$SK_B(X) = \bigcup_{n=0}^{\infty} SK_B^{(n)}(X), \quad (2)$$

where “ \setminus ” is the set difference operation, $0B$ is the singleton consisting of the origin, and

$$nB = \overbrace{B \oplus B \oplus \dots \oplus B}^{n \text{ times}}, \quad n = 1, 2, \dots$$

Moreover, the discrete image X can be reconstructed from its morphological skeleton by

$$X = \bigcup_{n=0}^{\infty} (\text{SK}_B^{(n)}(X) \oplus nB). \quad (3)$$

For each n , $\text{SK}_B^{(n)}(X)$ is the n th skeleton subset of X . If B is the unit disk centered at the origin, then $\text{SK}_B^{(n)}(X)$ consists of the centers of maximal disks in X with radius n .

The earlier morphological skeleton representation has been generalized to gray-scale images¹⁶ and l images.²³ In order to simplify its comparison with fuzzy medial axis transformation, we will make use of the following version of morphological skeletonization on gray-scale images proposed by Maragos and Schafer.¹⁶ First, for any gray-scale images $f, g: R^2 \rightarrow (0, 1, \dots, L)$, the image difference of f and g , written as $f \setminus g$, is defined by

$$(f \setminus g)(x) = \begin{cases} f(x) & \text{if } f(x) > g(x) \\ 0 & \text{otherwise} \end{cases}. \quad (4)$$

Then for a gray-scale image and a symmetrical flat structuring element B , define (For a gray-scale image f and a flat structuring element B , the dilation $f \oplus B$ and erosion $f \ominus B$ are defined by $(f \oplus B)(x) = \max_{q \in B} f(x - q)$ and $(f \ominus B)(x) = \min_{q \in B} f(x + q)$, respectively.)

$$\text{SK}_B^{(n)}(f) = (f \ominus nB) \setminus [(f \ominus nB) \circ B], \quad (5)$$

for $n = 1, 2, \dots$, and

$$\text{SK}_B(f) = \bigvee_{n=0}^{\infty} \text{SK}_B^{(n)}(f). \quad (6)$$

As in binary case, f can be reconstructed by

$$f = \bigvee_{n=0}^{\infty} (\text{SK}_B^{(n)}(f) \oplus nB). \quad (7)$$

For each n , $\text{SK}_B^{(n)}(f)$ is the n th skeletal subimage of f with respect to B . Usually, the symmetrical flat structuring element B is chosen to be the unit disk centered at the origin. In such case, we will simply denote the morphological skeleton and skeletal subimages of f by $\text{SK}(f)$ and $\text{SK}^{(n)}(f)$, $n = 0, 1, 2, \dots$, respectively. Note that for each n , the result $\text{SK}^{(n)}(f)(x) > 0$ indicates a maximal disk with radius n at level $\text{SK}^{(n)}(f)(x)$ and centered at x . Maximal disks with a common center can be stacked up to form a ‘‘morphological disk.’’ By a morphological disk, we mean a gray-scale image m such that the threshold set $m_t = \{x | f(x) \geq t\}$ is a disk for each gray level t . Then for each p in the support M_f of $\text{SK}(f)$, the morphological disk m_p^f can be obtained by

$$m_p^f = \bigvee_{n=0}^{\infty} (S_p^{(n)} \oplus nB), \quad (8)$$

where the image $S_p^{(n)}$ is defined to be

$$S_p^{(n)}(q) = \begin{cases} \text{SK}^{(n)}(f)(p) & \text{if } p = q \\ 0 & \text{otherwise} \end{cases}, \quad (9)$$

for each q in R^2 . Note that $\bigvee_{p \in M_f} S_p^{(n)} = \text{SK}^{(n)}(f)$ and $(m_p^f)_t = \bigcup_{n=0}^{\infty} [(S_p^{(n)})_t \oplus nB]$ is either an empty set or a disk for each gray level t . Further note that the image f can also be reconstructed from the morphological disks m_p^f , $p \in M_f$.

Proposition 1. Let M_f denote the support of $\text{SK}(f)$. Then f can be reconstructed from those morphological disks defined in Eq. (8), i.e., $f = \bigvee_{p \in M_f} m_p^f$.

Proof. From Eqs. (7) and (8), we have

$$\begin{aligned} \bigvee_{p \in M_f} m_p^f &= \bigvee_{p \in M_f} \bigvee_{n=0}^{\infty} (S_p^{(n)} \oplus nB) \\ &= \bigvee_{n=0}^{\infty} \bigvee_{p \in M_f} (S_p^{(n)} \oplus nB) \\ &= \bigvee_{n=0}^{\infty} ((\bigvee_{p \in M_f} S_p^{(n)}) \oplus nB) \\ &= \bigvee_{n=0}^{\infty} (\text{SK}^{(n)}(f) \oplus nB) \\ &= f. \end{aligned}$$

Thus, f can be reconstructed from m_p^f 's.

Example 1. Let f_1 be a one-dimensional signal given by

p	...	0	1	2	3	4	5	6	7	8	9	10	11	12	13	14	...
f_1	...	0	1	3	5	7	9	6	3	6	9	7	5	3	1	0	...

and let B be the flat structuring element given by $(-1, 0, 1)$. All the intermediate results needed to find the skeleton of f_1 are listed

p	...	0	1	2	3	4	5	6	7	8	9	10	11	12	13	14	...
$f_1 \ominus 0B$...	0	1	3	5	7	9	6	3	6	9	7	5	3	1	0	...
$(f_1 \ominus 0B) \circ B$...	0	1	3	5	6	6	6	3	6	6	6	5	3	1	0	...
$f_1 \ominus 1B$...	0	1	3	5	6	6	3	3	3	6	6	3	1	0
$(f_1 \ominus 1B) \circ B$...	0	1	3	3	3	3	3	3	3	3	3	3	1	0
$f_1 \ominus 2B$...	0	1	3	3	3	3	3	3	3	3	3	1	0
$(f_1 \ominus 2B) \circ B$...	0	1	3	3	3	3	3	3	3	3	3	1	0
$f_1 \ominus 3B$...	0	1	3	3	3	3	3	3	1	0
$(f_1 \ominus 3B) \circ B$...	0	1	3	3	3	3	3	3	1	0
$f_1 \ominus 4B$...	0	1	3	3	3	1	0
$(f_1 \ominus 4B) \circ B$...	0	1	3	3	3	1	0
$f_1 \ominus 5B$...	0	1	3	1	0
$(f_1 \ominus 5B) \circ B$...	0	1	1	1	0
$f_1 \ominus 6B$...	0	1	0
$(f_1 \ominus 6B) \circ B$...	0	0	0

The morphological skeletal subimages $\text{SK}_h^{(n)}(f_1)$ are obtained to be

p	...	0	1	2	3	4	5	6	7	8	9	10	11	12	13	14	...
$\text{SK}^{(0)}(f_1)$...	0	7	9	0	0	0	9	7	0
$\text{SK}^{(1)}(f_1)$...	0	5	6	0	0	0	6	5	0
$\text{SK}^{(5)}(f_1)$...	0	3	0
$\text{SK}^{(6)}(f_1)$...	0	1	0

Then the morphological disks of f_1 can be expressed as

p	...	0	1	2	3	4	5	6	7	8	9	10	11	12	13	14	...
m_4^f			...	0	5	7	5	0	...								
m_5^f				...	0	6	9	6	0	...							
m_7^f	...	0	1	3	3	3	3	3	3	3	3	3	3	3	1	0	...
m_9^f							...	0	6	9	6	0	...				
m_{10}^f								...	0	5	7	5	0	...			
$f_1 = \bigvee_{p \in M_{f_1}} m_p^f$...	0	1	3	5	7	9	6	3	6	9	7	5	3	1	0	...

2.2 Fuzzy-Medial-Axis Transformation (FMAT)

Based on the notion of fuzzy disks, Pal and Rosenfeld²¹ define FMAT for gray-scale images. FMAT generalizes the medial axis transformation for binary images to fuzzy subsets of a metric space. Let D be a metric space with metric d and let f be a fuzzy subset of D . For each $p \in D$, a fuzzy disk g_p^f centered at p is a fuzzy set defined by

$$g_p^f(q) \equiv \inf_{d(p,r)=d(p,q)} f(r). \tag{10}$$

Remind that a point $p \in D$ is called a local maximum of f if p has no neighbors q such that $g_p^f < g_q^f$. The fuzzy medial axis of f is defined by the set D_f of such local maxima of f , and $\{g_p^f | p \in D_f\}$ is called the FMAT of f .

One important property of FMAT is that the original image can be completely reconstructed from its FMAT. However, to record the FMAT information it needs a lot of memory, sometimes even more than to store the original image. Pal and Wang²² propose a redundant removal algorithm to tackle this problem. Their algorithm yields the so called reduced FMAT (RFMAT).

The FMAT has a ‘‘convex’’ definition, if we define the FMAT only using the maximal convex fuzzy disks. By a convex fuzzy disk, we mean a fuzzy disk g_p such that for all q_1, q_2 with $d(p,q_1) < d(p,q_2)$ we have $g_p(q_1) \geq g_p(q_2)$. Now, given an image f . For each $p \in D$, a convex fuzzy disk c_p^f centered at p is defined by

$$c_p^f(q) = \begin{cases} g_p^f(q) & \text{if } g_p^f(r) = \inf_{d(p,s) \leq d(p,r)} g_p^f(s), \\ & \forall r \text{ with } d(p,r) \leq d(p,q) \\ 0 & \text{otherwise} \end{cases}$$

Let C_f be the set of all $p \in D$ such that c_p^f are maximal among all convex fuzzy disks of f . Then the set C_f is called the convex fuzzy medial axis of f and $\{c_p^f | p \in C_f\}$ is called the convex fuzzy medial axis transformation (CFMAT) of f .

Proposition 2. All morphological disks of an image f are convex fuzzy disks.

Proof. Let m_p^f be a morphological disk of f centered at p . First, we note that for any points q_1 and q_2 with $d(p,q_1) < d(p,q_2)$, we have

$$\begin{aligned} m_p^f(q_1) &= \bigvee_{n=0}^{\infty} (S_p^{(n)} \oplus nB)(q_1) = SK^{d(p,q_1)}(p) \leq SK^{d(p,q_2)}(p) \\ &= \bigvee_{n=0}^{\infty} (S_p^{(n)} \text{bt}nB)(q_2) = m_p^f(q_2). \end{aligned}$$

This concludes that m_p^f is a convex fuzzy disk.

Since conventional and morphological disks are convex, in the rest of this paper, we will restrict our discussion on comparing MSK and CFMAT.

Example 1 (continued). The maximal fuzzy disks and maximal convex fuzzy disks for f_1 are

p	...	0	1	2	3	4	5	6	7	8	9	10	11	12	13	14	...
$g_p^f = f_1$...	0	1	3	5	7	9	6	3	6	9	7	5	3	1	0	...
c_4^f	...	0	1	3	5	7	5	3	1	0	...						
c_5^f	...	0	1	3	3	6	9	6	3	3	1	0	...				
c_9^f					...	0	1	3	3	6	9	6	3	3	1	0	...
c_{10}^f							...	0	1	3	5	7	5	3	1	0	...

3 Relations between Morphological Skeletonization and Fuzzy Medial Axis Transformation

Similarities between morphological skeletonization and FMAT are that (i) both of them are derived from the concept of ‘‘maximal disks;’’ (ii) both of them can be used to reconstruct the original image; and (iii) both the support of $SK(f)$ and the set C_f of an image f contain all the peaks of f . By a peak of f , we mean a pixel p such that $f(p) > f(q)$, for all $q (\neq p)$ in a neighborhood of p . Similarity (iii) can be shown as follows. Suppose there exists a peak p which does not belong to the CFMAT of f . Then there must exist a convex fuzzy disk c_q^f such that $c_q^f = (f(q), f(q_1), \dots, f(q_k) = f(p), \dots, f(q_n))$ for some integers k and n with $0 < k \leq n$. Let u be a neighbor of p with $d(q,u) = k - 1$. By the definition of convex fuzzy disks, $f(u) \geq f(q_{k-1}) \geq f(p)$. This contradicts to the assumption that p is a peak. Therefore, the set C_f contains all the peaks of f . Similarly, since morphological disks are convex, the set M_f also contains all the peaks of f .

However, there are some dissimilarities. First, the disks c_p^f 's in CFMAT are all maximal fuzzy convex disks, while the morphological disks m_p^f 's are not. For instance, in example 1, we have $m_5^f < c_5^f$. That is, m_5^f is not a maximal fuzzy convex disk. Next, the convex fuzzy medial axis transformation does not satisfy the ‘‘threshold-max superposition,’’ while the morphological skeletonization does.

Let Ψ be an operation on gray-scale images. For any binary image $A \subset R^2$, if we define

$$\chi_A(x) = \begin{cases} L & \text{if } x \in A \\ 0 & \text{otherwise} \end{cases}$$

then Ψ can be applied to binary images by defining

$$\Psi(A) \equiv \Psi(\chi_A).$$

Now, an operation Ψ on gray-scale images is said to satisfy the threshold-max superposition^{1,24,25} if for any gray-scale image f :

$$\Psi(f)(x) = \max\{t | x \in \Psi(f_t)\},$$

for all pixel x . Where $f_t = \{x | f(x) \geq t\}$ is the threshold set of f at level $t, t = 1, 2, \dots, L$. Before proving the following

proposition, we should note that for any sequence of gray-scale images $f_i, i \in I$:

$$\bigvee_{i \in I} f_i(x) = \max\{t | x \in \bigcup_{i \in I} (f_i)_t\}.$$

Proposition 3. The morphological skeletonization defined in formula (4)–(6) obeys the *threshold-max superposition*. That is

$$SK(f)(x) = \max\{t | x \in SK(f_t)\}.$$

Proof. First of all, we claim that $SK^{(n)}(f)(x) = \max\{t | x \in SK^{(n)}(f_t)\}$ for each n .

Let $SK^{(n)}(f)(x) = s$.

Case 1. Suppose $s = 0$. Then

$$(f \ominus nB)(x) = [(f \ominus nB) \circ B](x).$$

Let $(f \ominus nB)(x) = [(f \ominus nB) \circ B](x) = s'$. Then we observe that

$$x \in (f \ominus nB)_t \cap [(f \ominus nB) \circ B]_t, \text{ for all } 0 \leq t \leq s',$$

and

$$x \notin (f \ominus nB)_t \cup [(f \ominus nB) \circ B]_t, \text{ for all } t > s'.$$

Thus

$$x \notin (f \ominus nB)_t \setminus [(f \ominus nB) \circ B]_t, \text{ for all } t.$$

Since $(f \ominus nB)_t = (f_t \ominus nB)$ and $[(f \ominus nB) \circ B]_t = (f_t \ominus nB) \circ B$, we have

$$x \notin (f_t \ominus nB) \setminus [(f_t \ominus nB) \circ B] = SK^{(n)}(f_t), \text{ for all } t.$$

Therefore, $\max\{t | x \in SK^{(n)}(f_t)\} = 0 = SK^{(n)}(f)(x)$.

Case 2. Suppose $s > 0$. In this case, we have

$$(f \ominus B)(x) > [(f \ominus nB) \circ B](x) \text{ and } (f \ominus nB)(x) = s.$$

Let $[(f \ominus nB) \circ B](x) = u$. Then we observe that

$$x \in (f \ominus nB)_t \cap [(f \ominus nB) \circ B]_t, \text{ for all } 0 \leq t \leq u,$$

$$x \notin (f \ominus nB)_t \cup [(f \ominus nB) \circ B]_t, \text{ for all } t > s,$$

and

$$x \in (f \ominus nB)_t \text{ and } x \notin [(f \ominus nB) \circ B]_t, \text{ for all } u < t \leq s.$$

Thus

$$x \in (f \ominus nB)_t \setminus [(f \ominus nB) \circ B]_t, \text{ for all } u < t \leq s$$

and

$$x \notin (f \ominus nB)_t \setminus [(f \ominus nB) \circ B]_t, \text{ for all } t \leq u \text{ or } t > s.$$

In other words

$$\begin{aligned} \max\{t | x \in (f \ominus nB)_t \setminus [(f \ominus nB) \circ B]_t\} \\ = \max\{t | x \in (f_t \ominus nB) \setminus [(f_t \ominus nB) \circ B]_t\} \\ = \max\{t | x \in SK^{(n)}(f_t)\} = s. \end{aligned}$$

Therefore, we have

$$\max\{t | x \in SK^{(n)}(f_t)\} = [SK^{(n)}(f)](x)$$

$$x \in (f_t \ominus nB) \setminus [(f_t \ominus nB) \circ B], \text{ for all } u < t \leq s.$$

Combining the earlier two cases, we conclude that

$$SK^{(n)}(f)(x) = \max\{t | x \in SK^{(n)}(f_t)\}.$$

Next, since

$$\begin{aligned} SK(f)(x) &= \bigvee_{n=0}^{\infty} SK^{(n)}(f)(x) = \max\{t | x \in \bigcup_{n=0}^{\infty} SK^{(n)}(f_t)\} \\ &= \max\{t | x \in SK(f_t)\}, \end{aligned}$$

it follows that the morphological skeletonization MSK satisfies the threshold-max superposition.

Finally, let us revisit example 1 again. In there, we have $M_{f_1} = \{4, 5, 7, 9, 10\} \supset C_{f_1} = \{4, 5, 9, 10\}$. It seems that CFMAT of a gray-scale image contains fewer points than MSK does. Unfortunately, this is not true in general as the following example shows.

Example 2. Let f_2 be a one-dimensional signal given by

p	...	0	1	2	3	4	5	6	7	8	9	10	...
$f_2(p)$...	0	1	1	1	1	2	3	4	3	2	0	...

and let B be the structuring element same as given in example 1. Then using the same expression as example 1, the skeletal subimages are

p	...	0	1	2	3	4	5	6	7	8	9	10	...
$SK^{(0)}(f_2)$...	0	4	0	...	
$SK^{(1)}(f_2)$...	0	3	0	...	
$SK^{(2)}(f_2)$...	0	2	0	...	
$SK^{(4)}(f_2)$...	0	1	0	...			

The maximal morphological disks are

$$m_5^{f_2} = (1, 1, 1, 1, 1), \quad m_7^{f_2} = (4, 3, 2).$$

However, the maximal convex fuzzy disks for f_2 are

$$c_5^{f_2} = (2, 1, 1, 1, 1), \quad c_6^{f_2} = (3, 2, 1, 1), \quad f_7^{f_2} = (4, 3, 2).$$

Thus, in this example, we have $M_{f_2} = \{5, 7\} \subset C_{f_2} = \{5, 6, 7\}$.

4 Translations Between CFMAT and MSK

In the previous section, we discussed the relationship between FMAT and MSK. As we have known, both FMAT and MSK can be used to reconstruct a given image. Thus,

there exists an indirect transformation between CFMAT and MSK. It is then interesting to ask whether there exists a direct transformation from CFMAT to MSK or from MSK to CFMAT.

4.1 Construct MSK Using Convex Fuzzy Medial Axis Transformation

One of similarities mentioned in the beginning of the previous section is that both CFMAT and MSK contain all the peaks of an image f . In other words, all peaks are common skeleton points in the CFMAT and the MSK of an image f . Another observation is that MSK satisfies the threshold-max superposition. Then we can develop an algorithm to construct the MSK from convex fuzzy disk set. The main idea of this transformation algorithm is using the threshold-max superposition to decompose the image then compute the morphological skeleton points for each decomposed component. The algorithm is described as follows.

Algorithm A. Construct MSK from CFMAT.

Input. A convex maximum fuzzy disk set.

Step 1. Select the radius values that appear in the convex maximum fuzzy disk set. Then sort these values in descending order and store the result in a queue.

Step 2. If the queue is empty then stop.

Otherwise, remove a value r from the queue.

Step 3. Mark the points whose gray values are equal to r . The marked and unmarked areas may be treated as a binary image.

Step 4. Apply the distance transformation¹⁸ u to the binary image.

Step 5. Select the points with the maximum distance as morphological skeleton points. A point p with the local maximum distance $u(p)$ is a morphological skeleton point and belongs to the skeletal subimage $SK^{(u(p)^{-1})}$.

Step 6. For each convex fuzzy disk, change the value of marked points as its next radius value.

Step 7. Go to step 2.

The following example is a one-dimensional case for illustrating the operation in algorithm A.

Example 3. Let f_1 be a one-dimensional signal and B be the flat structuring element as given in example 1. The maximal convex fuzzy disks for f_1 are

$$c_4^{f_1} = (7, 5, 3, 1), \quad c_5^{f_1} = (9, 6, 3, 3, 1),$$

$$c_9^{f_1} = (9, 6, 3, 3, 1), \quad c_{10}^{f_1} = (7, 5, 3, 1).$$

Then the step-by-step process of algorithm A is illustrated in the following table.

p	...	0	1	2	3	4	5	6	7	8	9	10	11	12	13	14	...	
$c_4^{f_1} = (7, 5, 3, 1)$...	0	1	3	5	7	5	3	1	0	...							
$c_5^{f_1} = (9, 6, 3, 3, 1)$...	0	1	3	3	6	9	6	3	3	1	0	...					
$c_9^{f_1} = (9, 6, 3, 3, 1)$...	0	1	3	3	6	9	6	3	3	1	0	...	
$c_{10}^{f_1} = (7, 5, 3, 1)$...	0	1	3	5	7	5	3	1	0	...	
$SK^{(9)}(f_1)$								9			9							
	...	0	1	3	5	7	5	3	1	0	...							
	...	0	1	3	3	6	6	6	3	3	1	0	...					
					...	0	1	3	3	6	6	6	3	3	1	0	...	
							...	0	1	3	5	7	5	3	1	0	...	
$SK^{(7)}(f_1)$								7			7							
	...	0	1	3	5	5	5	3	1	0	...							
	...	0	1	3	3	6	6	6	3	3	1	0	...					
					...	0	1	3	3	6	6	6	3	3	1	0	...	
							...	0	1	3	5	5	5	3	1	0	...	
$SK^{(6)}(f_1)$								6			6							
	...	0	1	3	5	5	5	3	1	0	...							
	...	0	1	3	3	3	3	3	3	1	0	...						
					...	0	1	3	3	3	3	3	3	3	1	0	...	
							...	0	1	3	5	5	5	3	1	0	...	
$SK^{(5)}(f_1)$								5			5							
	...	0	1	3	3	3	3	3	1	0	...							
	...	0	1	3	3	3	3	3	3	1	0	...						
					...	0	1	3	3	3	3	3	3	3	1	0	...	
							...	0	1	3	3	3	3	3	1	0	...	
$SK^{(3)}(f_1)$								3			3							
	...	0	1	3	3	3	3	3	3	3	1	0	...					
	...	0	1	3	3	3	3	3	3	3	1	0	...					
					...	0	1	3	5	5	5	3	1	0	...			
$SK^{(1)}(f_1)$								1			1							
	...	0	1	1	1	1	1	1	1	1	1	1	1	1	1	1	0	...
$SK^{(0)}(f_1)$											1							

4.2 Construct CFMAT Using Morphological Skeleton

Although the MSK and CFMAT possess many common center points of the image and the CFMAT has been used to construct the MSK. However, to construct the CFMAT by MSK is not a straight forward. Since CFMAT is different

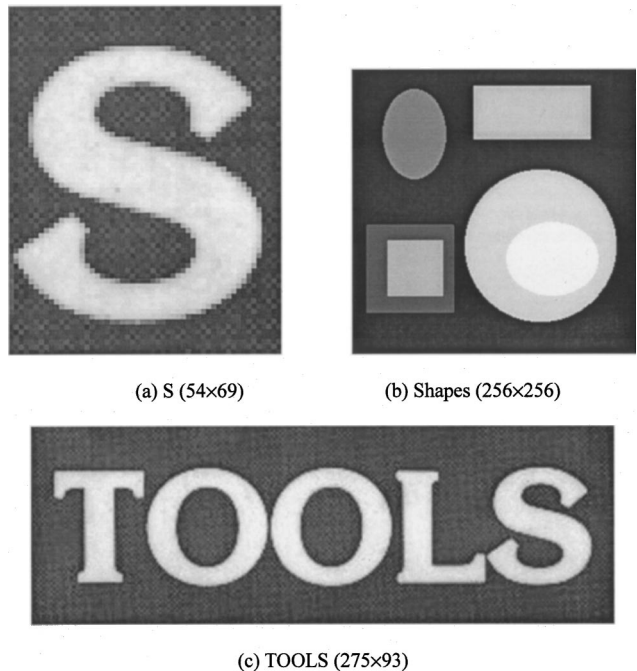


Fig. 1 Test images.

Table 1 Computation time and memory required for MSK.

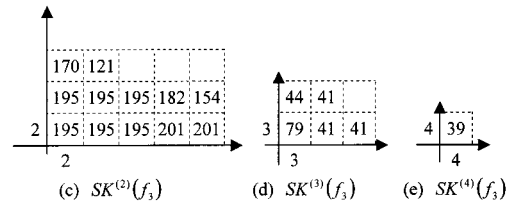
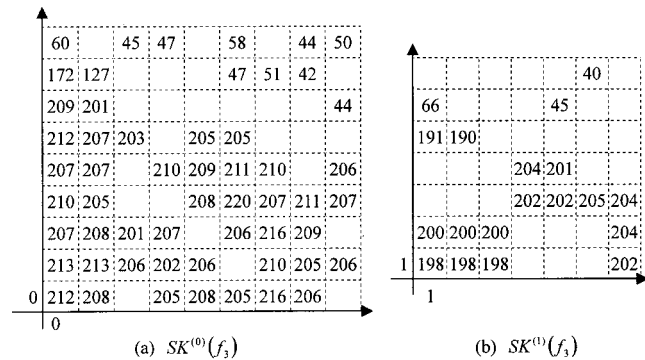
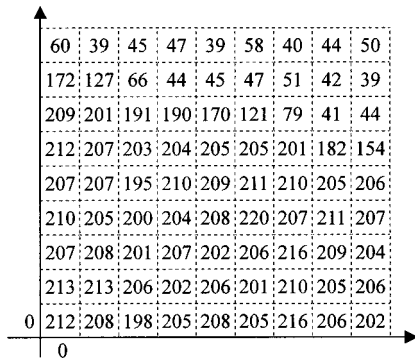
	# skeleton points	# gray values	Time used (s)
Shapes image	410	412	5.30
S image	2736	5021	0.17
Smoothed S image	1037	2024	0.17
TOOLS image	20 538	36 970	2.26
Smoothed TOOLS image	6987	12 277	2.28

Table 2 Time used for construct MSK from CFMAT.

	Time used for CFMAT (s)	Time used for MSK (s)	Total time used (s)
Shapes image	6.15	3.27	9.43
S image	0.16	1.51	1.67
Smoothed S image	0.60	1.28	1.88
TOOLS image	1.48	16.85	18.33
Smoothed TOOLS image	23.74	12.80	36.54

from MSK, one cannot expect to obtain the CFMAT just by using points in MSK. A concrete example is given as follows.

Example 4. Let f_3 be a two-dimensional signal given by



Using morphological skeletonization formula (3) and (4), the MSK of f_3 can be obtained. The skeletal subimages are

Note that the blank denotes that the pixel's gray value equal to 0. We construct maximal convex fuzzy disks cen-

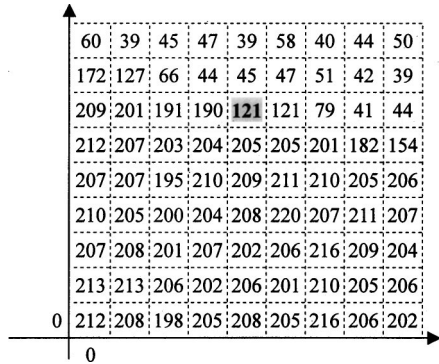
Table 3 Experiment results of the image S.

	FMAT	FMAT using convex disks CFMAT	RFMAT using convex disks	FMAT produced by algorithm B	FMAT produced by algorithm B + redundant removal algorithm
# fuzzy disk	3233	2609	2261	2508	2261
# gray values	36 145	11 431	9565	10 946	9564
Time used for FMAT or CFMAT			0.13 s	0.14 s	0.13 s
Time used for MSK				0.16 s	0.16 s
Time used for redundant removal			0.03 s		0.01 s
Total time used	1.40 s	0.14 s	0.16 s	0.30 s	0.30 s

Table 4 Experiment results of the image TOOLS.

	FMAT	FMAT using convex disks (CFMAT)	RFMAT using convex disks	FMAT produced by algorithm B	FMAT produced by algorithm B +redundant removal algorithm
# fuzzy disk	24 677	19 317	16 841	18 601	16 840
# gray values	532 444	80 646	67 855	77 230	67 846
Time used for FMAT or CFMAT			0.98 s	1.00 s	0.99 s
Time used for MSK				2.21 s	2.21 s
Time used for redundant removal			0.20 s		0.04 s
Total time used	81.51 s	1.00 s	1.20 s	3.23 s	3.26 s

tered at these points and use them to build an image. This built image is



We observe that the image we just built has gray value

121 at the point (4, 6) [the left down corner is the origin (0, 0)] while the original gray value at this point is 170.

To find a convex FMAT of an image, some points must be added to the set MSK for keeping the reconstruction property. Our approach is to check the sponsoring points for MSK points. The concept of sponsoring points is proposed by Pal and Wang,²² and used to check the redundancy fuzzy disks, originally. If every point in a fuzzy disk has more than one sponsoring point other than itself, then this fuzzy disk is redundant and can be removed from the FMAT. In the current study, we use this representation to check whether the point sponsored by the other points. Once the points without sponsoring point are found, we then find additional maximal convex fuzzy disks centered at these points. They, together with those centered at MSK points, form a CFMAT. This CFMAT can be further re-

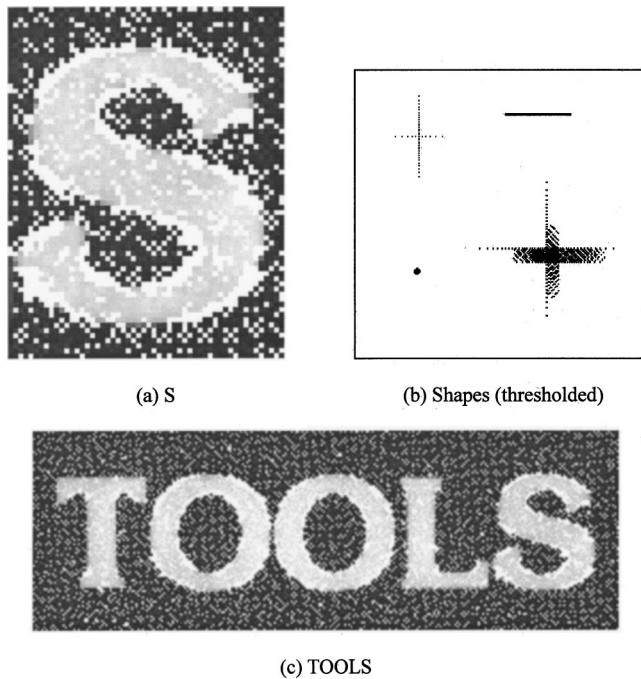


Fig. 2 Outputs of CFMAT.

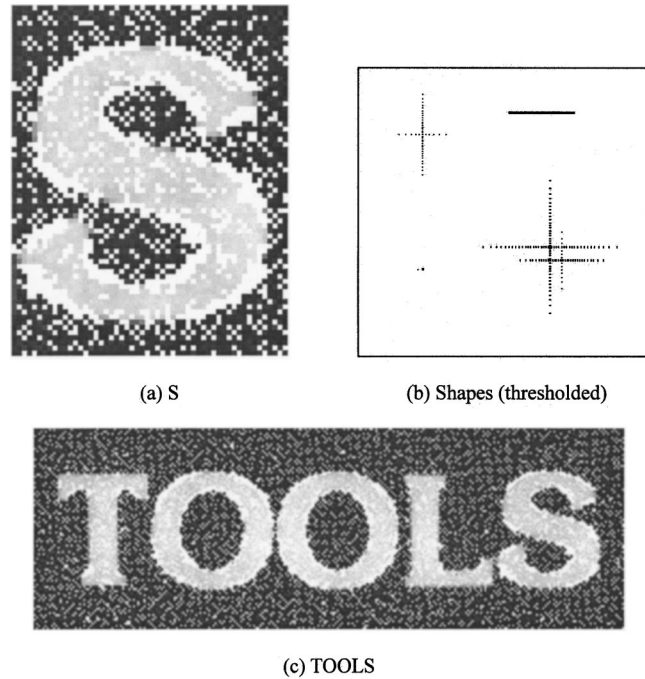


Fig. 3 Outputs of algorithm B.

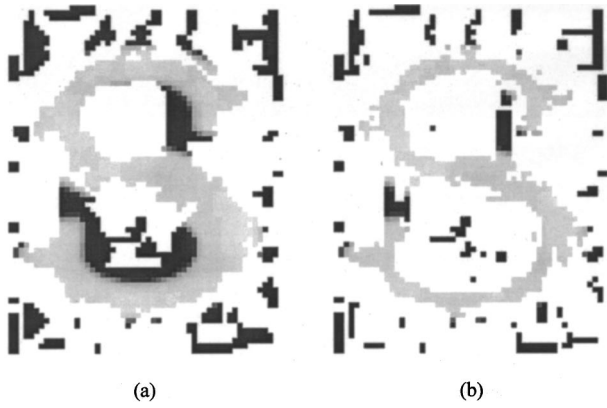


Fig. 4 RFMAT options.

duced by removing the redundant points. We summarize our approach in the following.

Algorithm B. Construct CFMAT from MSK.

Input. The morphological skeleton $SK(f)$. Let M_f be the support of $SK(f)$.

Step 1. Mark all morphological skeleton points $p \in M_f$ as the centers of the fuzzy disks.

Step 2. If all morphological skeleton points $p \in M_f$ are unmarked, then go to step 7. Otherwise, select one of marked skeleton point q and unmark it.

Step 3. Radius = - 1.

Step 4. Radius = radius + 1.

Step 5. If radius exceeds the object boundary then go to step 2.

Otherwise, compute the value

$$l = \min_{r \in [s|d(s,r)=radius]} \max\{SK^{(n)}(r) | n=0,1,2,\dots,N\}.$$

Step 6. If l less than the precedent one, then record l in the fuzzy disk center at q and go to step 4. Otherwise, go to step 2.

Step 7. Check each point in M_f and mark its sponsoring points. If there exist points with no sponsoring points, then add these points to the set M_f and find the corresponding convex fuzzy disks centered at them.

Step 8. (Inclusion detection) Check each p in M_f . If the fuzzy disk c_p^f is contained in another fuzzy disk c_q^f , then the point p is removed from M_f .

The set $\{c_p^f | p \in M_f\}$ is the desired CFMAT of f . This algorithm is essentially the same as the algorithm proposed by Pal and Wang except that we use morphological skeletal points to initialize an approximation for CFMAT.

Example 4. (continued) Note that the pixel (4, 6) has no sponsored points. Thus, we add (4, 6) to C_f and find the maximal fuzzy convex disk $c_{(4,6)}^f = (170,44,39)$.

Before ending this section, a one-dimensional example is used to illustrate the operation of algorithm B.

Example 5. Let f_1 be a one-dimensional signal and B be the flat structuring element as given in example 1. The morphological skeletal subimages for f_1 are shown in example 1.

p	...	0	1	2	3	4	5	6	7	8	9	10	11	12	13	14	...
$SK^{(0)}(f_1)$...	0	7	9	0	0	0	9	7	0	...		
$SK^{(1)}(f_1)$...	0	5	5	5	0	0	0	5	5	5	0	...		
$SK^{(2)}(f_1)$...	0	6	6	6	0	6	6	6	0	...			
$SK^{(5)}(f_1)$...	0	3	3	3	3	3	3	3	3	3	3	3	0	...	
$SK^{(6)}(f_1)$...	0	1	1	1	1	1	1	1	1	1	1	1	1	1	0	...

The translation results are

$$c_4^{f_1} = (7,5,3,1), \quad c_5^{f_1} = (9,6,3,3,1),$$

$$c_9^{f_1} = (9,6,3,3,1), \quad c_{10}^{f_1} = (7,5,3,1).$$

Based on algorithm B, we choose all of the morphological skeletal points as centers of the fuzzy disks. Then we sequentially check the radii to search the minimum gray values. For example, the coordinate 4 is a morphological

Table 5 Experiment results of the smoothed image S.

	FMAT	FMAT using convex disks (CFMAT)	RFMAT using convex disks	FMAT produced by algorithm B	FMAT produced by algorithm B + redundant removal algorithm
# fuzzy disk	1936	1573	602	966	602
# gray values	27 425	18 693	6202	10 752	6169
Time used for FMAT or CFMAT			0.54 s	0.23 s	0.24 s
Time used for MSK				0.16 s	0.16 s
Time used for redundant removal			0.98 s		0.15 s
Total time used	0.92 s	0.54 s	1.52 s	0.39 s	0.55 s

Table 6 Experiment results of the smoothed image TOOLS.

	FMAT	FMAT using convex disks (CFMAT)	RFMAT using convex disks	FMAT produced by algorithm B	FMAT produced by algorithm B+redundant removal algorithm
# fuzzy disk	14 112	11 503	3101	6412	3075
# gray values	36 998	216 152	51 083	118 979	50 503
Time used for FMAT or CFMAT			18.04 s	5.76 s	5.65 s
Time used for MSK				2.21 s	2.21 s
Time used for redundant removal			46.08 s		7.01 s
Total time used	46.06 s	18.09 s	64.13 s	8.00 s	14.88 s

skeletal point, and is selected as the center of a fuzzy disk. The minimum gray values corresponding to radii 1, 2, 3 are 5, 3, 1, respectively. The search for minimum gray values is finished when the radius equal to 4 which exceeds the distance from point 4 to the object boundary. Thus, the convex fuzzy disk center at 4 is $c_4^f = (7,5,3,1)$.

5 Experimental Results and Discussions

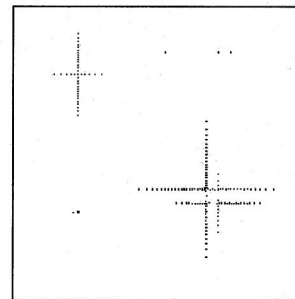
For demonstrating the proposed methods, we apply them to the test images presented in Fig. 1. The sizes of test images "S," "Shapes," and "TOOLS" are 54×69 , 256×256 , and 275×93 , respectively. All of them are 8-bits gray level images. The Shapes is a synthesis image. The gray values of the background are 0, the ellipse at the up-left corner are 100, the rectangle are 180, the outer square at the left-bottom corner are 60, the inner square at the same corner are 160, the circle are 200, and the ellipse inside the circle are 230. The simulation programs are written in C language and run on a Pentium II 300 over clock to 450 PC.

In the experiments, we observed that the computation times for MSK are less than the CFMAT, and MSK can be obtained from the CFMAT using algorithm A proposed in Sec. 4.1. Table 1 presents the computation time, number of skeleton points, and storage required for the morphological



(a) "S"

(b) Smoothed "S"



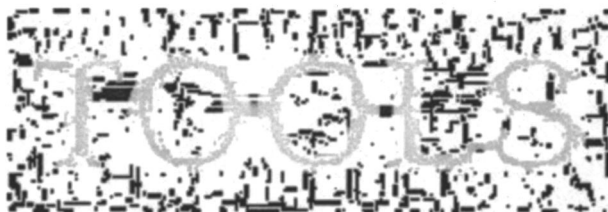
(c) "Shapes" (thresholded)



(a)



(d) "TOOLS"



(b)



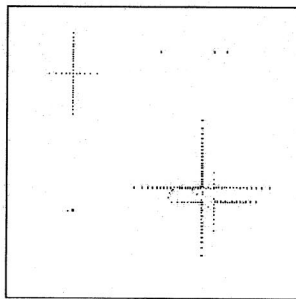
(e) Smoothed "TOOLS"

Fig. 5 (a) CFMAT output of smoothed image S; (b) output of smoothed image S derived from algorithm B.

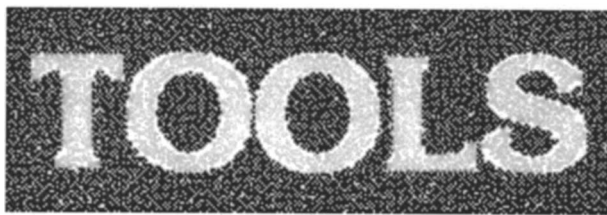
Fig. 6 (a) CFMAT output of smoothed image TOOLS; (b) output of smoothed image TOOLS derived from algorithm B.



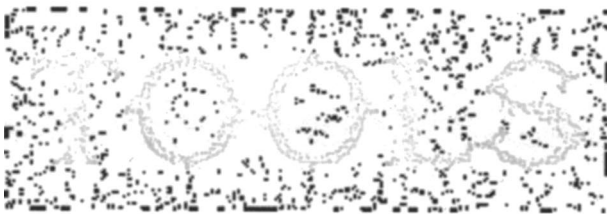
(a) "S" (b) Smoothed "S"



(c) "Shapes" (thresholded)



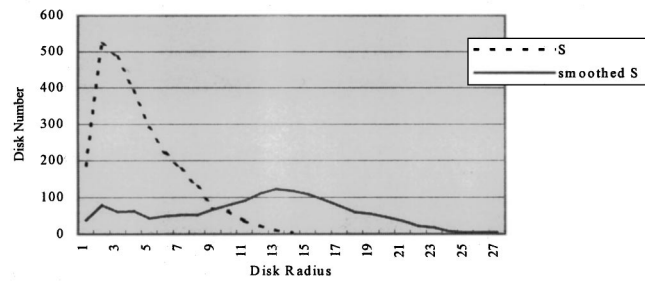
(d) "TOOLS"



(e) Smoothed "TOOLS"

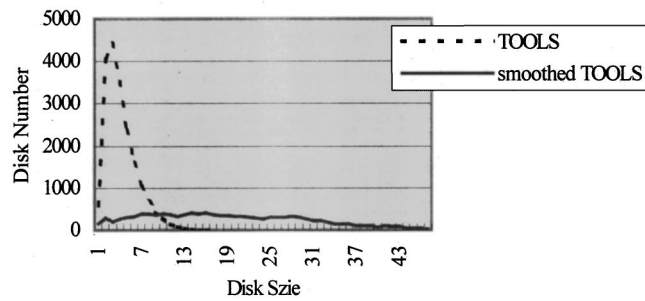
Fig. 7 Fuzzy disk size distribution for CFMAT.

Fuzzy Disk Size Distribution (CFMAT)



(a)

Fuzzy Disk Size Distribution (CFMAT)



(b)

Fig. 8 Outputs derived from combination of algorithm B and redundant removal algorithm.

skeletonization of each image. In this case, we have to record the indexes of the morphological skeleton subsets for each gray value in MSK. For example, the results of the morphological skeletonization of image S are 410 skeleton points and 412 gray values accompany with 412 indexes of skeleton subsets. The experiment results of algorithm A are shown in Table 2. According with these experimental results, algorithm A spends more time to construct MSK from the CFMAT than to compute MSK from the original image directly. Thus, we will concentrate our discussion on algorithm B proposed in section 4-2.

Tables 3 and 4 present the experimental results of the test images. For the image S, the skeleton points (i.e., centers of disks) produced by morphological skeletonization are 2736 points (see Table 1). The output of algorithm B is 2508 points. The size of the CFMAT yielded by the method

Table 7 Experiment results of the image Shapes.

	FMAT	FMAT using convex disks(CFMAT)	RFMAT using convex disks	FMAT produced by algorithm B	FMAT produced by algorithm B+redundant removal algorithm
# fuzzy disk	1100	1100	238	410	238
# gray values	37 213	37 213	6979	11 936	6967
Time used for FMAT or CFMAT			4.91 s	1.28 s	1.28 s
Time used for MSK				5.18 s	5.18 s
Time used for redundant removal			97.25 s		3.46 s
Total time used	4.90 s	4.89 s	102.17 s	6.48 s	9.43 s

of Pal and Wang²¹ is 2609 and the number of recorded gray values is 11431. Figures 2 and 3 present the results of CFMAT and algorithm B, respectively. The RFMAT output is 2261 points (disks) and 9565 gray values. The RFMAT outputs of test images and their smoothed versions are shown in Fig. 4. Algorithm B combines the redundant removal algorithm yields 2261 fuzzy disks and records 9564 gray values. For this image, the experiment results reveal that the method of Pal and Wang²¹ is faster than algorithm B, even when the redundant removal algorithm is applied. The outputs of both methods are almost the same after the redundant removal algorithm is applied. Analogy results for the image TOOLS are shown in Table 4. It should be noted that the output images just present the skeleton points. Each skeleton point keeps the original gray value, and the non-skeleton point presents the blank. For the sake of clarity, the image S and the results of the image S are enlarged five times of their original sizes. The results of the Shapes image are thresholded for the same reason.

For smoothed images, the computation time increases in the method of Pal and Wang. Tables 5 and 6 show the experiment results for this situation. The outputs of CFMAT and algorithm B for the smoothed test images are shown in Figs. 5 and 6, respectively. A smooth area in the image will result in a large disk. For example, the radius of the largest fuzzy disk found by CFMAT in the image S is 14 while that is 27 in the smoothed version. Figure 7 presents the convex fuzzy disk size distributions of the S and TOOLS, and their smoothed images. It confirms that smooth areas trend to produce larger convex fuzzy disks. Then the method of Pal and Wang has to spend more computation time for disk inclusion detection. Hence, in the case of smoothed images, algorithm B is usually faster than their method. This conclusion is confirmed again by the experiment results of the image Shapes shown in Table 7. The time used for RFMAT is longer than the others. Most of the time is spent in the redundant removal algorithm, since it checks a large amount of points for each 1100 disks.

We then apply the redundant removal algorithm²² to the output of algorithm B. The experiment results for this situation are shown in Fig. 8. Although it requires more computation time than the method of Pal and Wang for test images, it requires less for the smoothed images. The experiment results reveal that the combination algorithm B and the redundant removal algorithm is effective for both original and smoothed image. For smoothed images, this combination is especially fast.

6 Conclusions

In this paper, we discuss the similarities and dissimilarities of MSK and FMAT and propose two algorithms to translate between CFMAT and MSK. The MSK of an image can be constructed by the CFMAT. However, the CFMAT cannot always be constructed solely by the MSK. Fortunately, with the help of the concept of the sponsor, we can construct CFMAT from the MSK with adding the points without sponsored points. The computation time of the method proposed by Pal and Wang depends on the sizes of smooth regions in an image, however, that of MSK depends only on the image size. Thus, algorithm B is very effective for smoothed images. The experimental results also reveal that

the combination of algorithm B and the redundant removal algorithm can produce the convex FMAT for test images and their smoothed versions, effectively.

References

1. J. Serra, *Image Analysis and Mathematical Morphology*, Academic, London (1982).
2. D. Shinha, P. Shinha, E. R. Dougherty, and S. Batman, "Design and analysis of fuzzy morphological algorithms for image processing," *IEEE Trans. Fuzzy Syst.* **5**(4), 570–584 (1997).
3. C. V. Jawahar and A. K. Ray, "Fuzzy statistics of digital images," *IEEE Signal Process. Lett.* **3**(8), 225–227 (1996).
4. *Fuzzy Models for Pattern Recognition*, J. C. Bezdek and S. K. Pal, Eds., IEEE, New York (1992).
5. F. Russo, "A new class of fuzzy operators for image processing: Design and implementation," in *Second IEEE Int. Conf. Fuzzy Systems*, Vol. 2, pp. 815–820, San Francisco, California (Mar. 28–Apr. 1, 1993).
6. F. Russo and G. Ramponi, "Nonlinear fuzzy operators for image processing," *Signal Process.* **38**(3), 429–440 (1994).
7. Y. G. Lee and Y. C. Hsueh, "Fuzzy logic approach for removing noise," *Neural Comput.* **9**(3), 349–355 (1995).
8. Y. G. Lee, J. H. Lee, and Y. C. Hsueh, "Fuzzy uncertainty texture spectrum for texture analysis," *Electron. Lett.* **31**(12), 959–960 (1995).
9. Y. G. Lee and Y. C. Hsueh, "Detail preserving image smoothing by mathematical morphology and fuzzy reasoning," *J. Electron. Imaging* **5**(3), 396–401 (1996).
10. D. Sinha and E. R. Dougherty, "Fuzzy mathematical morphology," *J. Visual Commun. Image Represent* **3**(3), 286–302 (1992).
11. D. Sinha and E. R. Dougherty, "A general axiomatic theory of intrinsically fuzzy mathematical morphologies," *IEEE Trans. Fuzzy Syst.* **3**(4), 389–403 (1995).
12. I. Bloch and H. Maitre, "Fuzzy mathematical morphologies: A comparative study," *Pattern Recogn.* **28**(9), 1341–1387 (1995).
13. T. Motzkin, "Sur quelques propriétés caractéristiques des ensembles bornés non convexes," *Atti Accad. Naz. Lincei, Cl. Sci. Fis., Mat. Nat., Rend.* **21**, 773–779 (1935).
14. C. Lantuéjoul, "La squelettisation et son application aux mesures topologiques des mosaïques polycristallines," PhD thesis, Paris, Paris School of Mines (1978).
15. P. A. Maragos and R. W. Schafer, "Morphological skeleton representation and coding of binary images," *IEEE Trans. Acoust., Speech, Signal Process.* **34**(5), 1228–1244 (1986).
16. P. A. Maragos, "A unified theory of translation-invariant systems with applications to morphological analysis and coding of images," PhD thesis, Georgia Institute of Technology (1985).
17. R. M. Haralick and L. G. Shapiro, *Computer and Robot Vision*, Vol. I, Addison-Wesley, Reading, Massachusetts (1992).
18. A. K. Jain, *Fundamentals of Digital Image Processing*, Prentice-Hall, Englewood Cliffs, New Jersey (1989).
19. J. M. Reinhardt and W. E. Higgins, "Comparison between the morphological skeleton and morphological shape decomposition," *IEEE Trans. Pattern Anal. Mach. Intell.* **18**(9), 951–957 (1996).
20. R. Kresch, "Morphological image representation for coding applications," PhD thesis, Israel Institute of Technology (1995).
21. S. K. Pal and A. Rosenfeld, "A fuzzy medial axis transformation based on fuzzy disks," *Pattern Recogn. Lett.* **12**, 585–590 (1991).
22. S. K. Pal and L. Wang, "Fuzzy medial axis transformation (FMAT): Practical feasibility," *Fuzzy Sets Syst.* **50**, 15–34 (1992).
23. S. R. Jan and Y. C. Hsueh, "Morphological skeletonization on *l*-images," in *Proc. CVGIP'96*, pp. 47–52, Taiwan, R.O.C. (1996).
24. P. Maragos and R. D. Ziff, "Threshold superposition in morphological image analysis systems," *IEEE Trans. Pattern Anal. Mach. Intell.* **12**(5), 498–504 (1990).
25. J. L. Davidson, "Thinning and skeletonizing," *Digital Image Processing Methods*, E. R. Dougherty, Ed., Marcel Dekker, New York (1994).



morphology, image processing, and pattern recognition.

Sen-Ren Jan received his BS degree in computer science from Tamkang University, Taipei, Taiwan, in 1983 and his MS, PhD degree in computer and information science from National Chiao Tung University, Hsinchu, Taiwan, in 1991, 2000, respectively. He is currently an assistance professor in the Department of Information Management at Ming Hsing Institute of Technology, Hsinchu, Taiwan. His current research interests include mathematical



Yuang-Cheh Hsueh received his BS degree in applied mathematics from National Chiao Tung University in 1976 and PhD degree in mathematics from UCLA in 1983. Currently, he is a professor in the Department of Computer and Information Science at National Chiao Tung University. His current research and teaching interests lie mainly in computer graphics, mathematical morphology, image algebra, and fuzzy set theory.